Quantum critical behavior in a graphenelike model

Simon Hands[1] and Costas Strouthos[2]
[1]*Department of Physics, Swansea University, Singleton Park, Swansea SA2 8PP, United Kingdom*
[2]*Department of Mechanical Engineering, University of Cyprus, Nicosia 1678, Cyprus*
(Received 4 July 2008; published 24 October 2008)

We present the results of numerical simulations of a (2+1)-dimensional fermion field theory based on a recent proposal for a model of graphene consisting of N_f four-component Dirac fermions moving in the plane and interacting via an instantaneous Coulomb interaction. In the strong-coupling limit we identify a critical number of flavors $N_{fc}=4.8(2)$ separating an insulating from a conducting phase. This transition corresponds to the location of a quantum critical point, and we use a fit to the equation of state for the chiral order parameter to estimate the critical exponents. Next we simulate $N_f=2$ corresponding to real graphene and approximately locate a transition from strong- to weak-coupling behavior. Strong correlations are evident in the weak-coupling regime.

DOI: 10.1103/PhysRevB.78.165423 PACS number(s): 73.63.Bd, 71.10.Fd, 11.10.Kk, 11.15.Ha

I. INTRODUCTION

While there has been considerable recent interest in graphene sparked by its discovery and subsequent experimental study,[1] the remarkable properties of electronic systems on two-dimensional honeycomb lattices have been suspected for many years.[2] In brief, for a carbon monolayer having one mobile electron per atom, a simple tight-binding model shows that the spectrum of low-energy excitations exhibits a linear dispersion relation centered on zeros located at the six corners of the first Brillouin zone (e.g., Ref. 3). Using a linear transformation among the fields at two independent zeros it is possible to recast the Hamiltonian in Dirac form with $N_f=2$ flavors of four-component spinor ψ—the counting of the massless degrees of freedom coming from two C atoms per unit cell times two zeros per zone times two physical spin components per electron. Electron propagation in the graphene layer is thus relativistic, albeit at a speed of $v_F \approx c/300$. The implication for the high mobility of the resulting charge carriers (which may be negatively charged "particles" or positively charged "holes" depending on doping) is the source of the current excitement. The stability of the zero-energy points is topological in origin as emphasized in Ref. 4.

While the above considerations apply quite generally, a realistic model of graphene must incorporate interactions between charge carriers. One such model due to Son[5] has N_f massless fermion flavors propagating in the plane but interacting via an instantaneous $3d$ Coulomb interaction. In Euclidean metric and static gauge $\partial_0 A_0=0$ the action reads

$$S_1 = \sum_{a=1}^{N_f} \int dx_0 d^2x (\bar{\psi}_a \gamma_0 \partial_0 \psi_a + v_F \bar{\psi}_a \vec{\gamma}.\vec{\nabla}\psi_a + iV\bar{\psi}_a\gamma_0\psi_a) + \frac{1}{2e^2}\int dx_0 d^3x (\partial_i V)^2, \quad (1)$$

where e is the electron charge, $V \equiv A_0$ is the electrostatic potential, and the 4×4 Dirac matrices satisfy $\{\gamma_\mu,\gamma_\nu\}=2\delta_{\mu\nu}$ with $\mu=0,1,2,3$. In our notation $\vec{x}$ is a vector in the $2d$ plane while the index i runs over all three spatial directions. Within the graphene layer, classical propagation of the potential is obtained by integrating over the perpendicular coordinate, yielding

$$D_0(p) = \frac{e^2}{2|\vec{p}|}. \quad (2)$$

To proceed, assume a large-N_f limit so that the dominant quantum correction $\Pi(p)$ comes from a vacuum polarization fermion—antifermion loop. The resummed V propagator becomes

$$D_1(p) = [D_0^{-1}(p) - \Pi(p)]^{-1} = \left[\frac{2|\vec{p}|}{e^2} + \frac{N_f}{8}\frac{|\vec{p}|^2}{(p^2)^{1/2}}\right]^{-1}, \quad (3)$$

where $p^2=(p_0,\vec{p})^2 \equiv p_0^2+v_F^2|\vec{p}|^2$. In either the strong-coupling or large-N_f limits $D_1(p)$ is thus dominated by the quantum correction—the relative importance of the original Coulomb interaction being governed by a parameter $\lambda \equiv |\Pi/D_0|_{p_0=0}$. Restoring international system (SI) of units, we obtain

$$\lambda = \frac{e^2 N_f}{16\varepsilon_0 \hbar v_F} \simeq 1.7 N_f. \quad (4)$$

The form of interaction (3) means that analytic methods are trustworthy in the large-N_f regime. For instance, in the strong-coupling limit $e^2\to\infty$ (in experiments it is only possible to *reduce* the effective electron charge by mounting the graphene layer on a dielectric substrate) we expect a modification of the dispersion relation such that the fermion energy is related to momentum via $\omega \propto p^z$, where z is a dynamical critical exponent predicted to take the value $z \simeq 1-\frac{4}{\pi^2 N_f} \approx 0.8$ for $N_f=2$.[5] Reference 5 in addition discusses the phase diagram of graphene model (1) in the (N_f,e^{-2}) plane and raises the possibility of symmetry breaking due to nonperturbative N_f^{-1} effects. The symmetry breaking, due to the spontaneous condensation of particle-hole pairs, is signaled by an order parameter $\langle\bar{\psi}\psi\rangle \neq 0$—in relativistic field theory this is known as "chiral symmetry breaking." Physically the most important outcome is the generation of a gap in the fermion spectrum implying that the model describes an insulator. Son postulated that this insulating phase exists in the corner of the phase diagram corresponding to large e^2 and small N_f,

and in particular, that the insulator-conductor phase transition taking place at $N_f=N_{fc}$ in the strong-coupling limit $e^2\to\infty$ is a novel quantum critical point. It is important to stress that, while we have followed Son's work closely in this presentation, many of the important features of this model such as the instantaneous interaction, the role of the vacuum polarization $\Pi(p)$, the possibility of spontaneous symmetry breaking via condensation of particle-hole pairs, and the nature of the phase diagram in the (N_f,e^{-2}) plane were first obtained in Refs. 6. The value of N_{fc}, and the issue of whether it is greater than or less than the physical value $N_f=2$, must be settled by a nonperturbative calculation. Recent estimates have been obtained by: self-consistent solution of the Schwinger-Dyson equation for the gap[6] yielding $N_{fc}=2.55$; and by a renormalization-group treatment of radiatively induced four-fermion contact interactions[7] yielding $N_{fc}=2.03$.

The proposed physics is very reminiscent of another $2+1d$ fermion model, this time relativistically covariant, namely, the Thirring model with action

$$S_{Th}=\sum_{a=1}^{N_f}\int dx_0d^2x\left[\bar{\psi}_a\gamma_\mu\partial_\mu\psi_a+\frac{g^2}{2}(\bar{\psi}_a\gamma_\mu\psi_a)^2\right], \quad (5)$$

with $\mu=0,1,2$—particularly once we insist on units such that $v_F=1$. Note that in contrast to the graphene model the coupling g^2 has mass dimension of -1. Once again, the model is analytically tractable at large N_f but exhibits spontaneous chiral symmetry breaking leading to gapped fermions at small N_f and large g^2.[8,9] Arguably the Thirring model is the simplest field theory of fermions requiring a computational solution: the location of the phase transition at $N_f=N_{fc}$ in the strong-coupling limit has recently been determined by lattice simulation to be $N_{fc}=6.6(1)$.[10] The apparent similarity of the two systems has led us to propose a Thirring-type model pertinent to graphene, with action

$$S_2=\sum_{a=1}^{N_f}\int dx_0d^2x\left[\bar{\psi}_a\gamma_\mu\partial_\mu\psi_a+\frac{g^2}{2}(\bar{\psi}_a\gamma_0\psi_a)^2\right]. \quad (6)$$

The only difference with Eq. (5) is that the contact interaction is now only between the timelike components of the fermion current so that the model is no longer covariant.

The traditional way to proceed is to introduce an auxiliary boson field V. The resulting action

$$S_2'=\sum_{a=1}^{N_f}\int dx_0d^2x\left[\bar{\psi}_a\gamma_\mu\partial_\mu\psi_a+iV\bar{\psi}_a\gamma_0\psi_a+\frac{1}{2g^2}V^2\right] \quad (7)$$

reproduces the identical dynamics as Eq. (6) once V is integrated out. As for Eq. (1) we assume a large-N_f limit to estimate the dominant vacuum polarization correction; the resultant propagator for V is

$$D_2(p)=\left(\frac{1}{g^2}+\frac{N_f}{8}\frac{|\vec{p}|^2}{(p^2)^{1/2}}\right)^{-1}. \quad (8)$$

In the strong-coupling or large-N_f limits, D_2 coincides with D_1 of Eq. (3), implying that the fermion interactions are equivalent. It is also the case that $\lim_{p\to\infty}D_2(p)=\lim_{\lambda\to\infty}D_1(p)$. This last limit is important because critical behavior in the Thirring model (5) is governed by a UV-stable fixed point of the renormalization group.[8] We anticipate that model (6) is similar and expect its predictions, in particular for critical behavior such as the value of N_{fc}, to be generally valid for Son's model (1) in the limit of large λ.

In Sec. II we present a version of action (7) discretized on a spacetime lattice and outline how its dynamics can be investigated by standard Monte Carlo simulation techniques. This paper applies lattice gauge theory techniques to graphene. In this first paper we focus exclusively on the equivalent of the order parameter $\langle\bar{\psi}\psi\rangle$ in the (N_f,g^{-2}) plane. In Sec. III A we explore the strong-coupling limit and identify the critical flavor number N_{fc} and then attempt to characterize the transition from insulator to conductor by studying the critical equation of state using finite-volume scaling (FVS). In Sec. III B we switch attention to the physical case $N_f=2$ and present results from a study of $\langle\bar{\psi}\psi\rangle$ as a function of g^2. A brief discussion of the implications for the graphene model of Ref. 5 follows.

II. LATTICE MODEL AND SIMULATION

The lattice model studied in this paper is closely related to the lattice Thirring model studied in Ref. 8. It is written in terms of staggered lattice fermions, i.e., single-component Grassmann fields $\chi,\bar{\chi}$ defined on the sites x of a three-dimensional cubic lattice, by the action

$$S_{\text{latt}}=\frac{1}{2}\sum_{x\mu a}\bar{\chi}_{ax}\eta_{\mu x}\left[\left(1+\delta_{\mu 0}\sqrt{\frac{2g^2}{N}}e^{iV_x}\right)\chi_{ax+\hat{\mu}}-\left(1+\delta_{\mu 0}\sqrt{\frac{2g^2}{N}}e^{-iV_{x-\hat{0}}}\right)\chi_{ax-\hat{\mu}}\right]+m\sum_{xa}\bar{\chi}_{ax}\chi_{ax}. \quad (9)$$

The flavor indices are $a=1,\ldots,N$. The sign factors $\eta_{x\mu}\equiv(-1)^{x_0+\cdots+x_{\mu-1}}$ ensure that in the long-wavelength limit the first (anti-Hermitian) term in S_{latt} describes the Euclidean propagation of $N_f=2N$ flavors of relativistic fermion described by four-component spinors.[11] The fermion mass term proportional to m has been added to provide an IR regulator for modes which would otherwise be massless; beyond the usual critical slowing down, it is important to stress that simulations directly in the limit $m\to 0$ present severe technical difficulties. The hopping terms in S_{latt} involve the auxiliary boson field V_x which is formally defined on the *timelike* links connecting sites x with $x+\hat{0}$. The N dependence in the kinetic terms is conventional and retained to ensure continuity with the studies of Refs. 8–10. In order to compare with the formulation of Sec. I the rescaling $g^2\to Ng^2$ is required.

It can be shown that action (9) can be re-expressed in terms of four-component spinors in a form similar but not identical to Eq. (6). For full details of the relation between the two actions we refer the reader to Ref. 8. Here we merely note that the spontaneous generation of a condensate $\langle\bar{\chi}\chi\rangle\neq 0$ in the lattice model results in a chiral symmetry-breaking pattern $\mathrm{U}(N)\otimes\mathrm{U}(N)\to\mathrm{U}(N)$, whereas in continuum model (6) $\langle\bar{\psi}\psi\rangle\neq 0$ breaks $\mathrm{U}(2N_f)\to\mathrm{U}(N_f)\otimes\mathrm{U}(N_f)$.[3] A term pro-

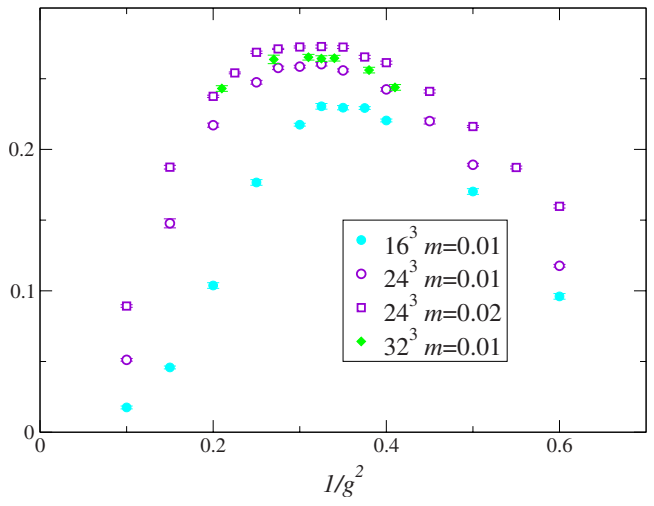

FIG. 1. (Color online) $\langle\bar{\chi}\chi\rangle$ vs $1/g^2$ for $N_f=2$.

portional to m explicitly breaks the symmetry in either case. It is plausible that the effective global symmetry of the lattice model enlarges in the continuum limit and the correct continuum pattern recovered. In what follows we will assume that the chiral symmetry breaking described by $\langle\bar{\chi}\chi\rangle \neq 0$ is equivalent to the metal-insulator transition.

The novelty of Ref. 10 was the first study of Thirring model (5) by lattice means in the strong-coupling limit $g^2 \to \infty$. Since we aim to repeat the strategy here we discuss how this was done. First, note that the vacuum polarization calculation leading to results (3) and (8) does not go through in quite the same way for lattice regularized model (9); rather, there is an additive correction which is momentum independent and UV divergent,

$$\Pi^{\text{latt}}(p) = \Pi^{\text{cont}}(p) + g^2 J(m), \tag{10}$$

where $J(m)$ comes from incomplete cancellation of a lattice tadpole diagram.[8] This extra divergence (not present in the continuum treatments) can be absorbed by a wave-function renormalization of V and a coupling-constant renormalization

$$g_R^2 = \frac{g^2}{1 - g^2 J(m)}. \tag{11}$$

In the large-N_f limit we thus expect to find the strong-coupling limit of the lattice model at $g_R^2 \to \infty$ implying $g^2 \to g_{\text{lim}}^2 = J^{-1}(m)$. For $g^2 > g_{\text{lim}}^2$, $D_{\text{latt}}(p)$ becomes negative, and S_{latt} no longer describes a unitary theory.

Away from the large-N_f limit, where chiral symmetry may be spontaneously broken, there is no analytical criterion for identifying g_{lim}^2; however, in this case a numerical calculation of $\langle\bar{\chi}\chi\rangle$ shows a clear peak at $g^2 = g_{\text{peak}}^2$, whose location is approximately independent of both volume and m, indicating an origin at the UV scale.[10] Figure 1 exemplifies this behavior in model (9) with $N_f=2$ on system volumes L^3: for $L \geq 24$ we identify $1/g_{\text{peak}}^2 \simeq 0.3$. Since for orthodox chiral symmetry breaking the magnitude of the condensate is expected to increase monotonically with the coupling strength, we interpret the peak as the point where unitarity violation sets in, i.e., $g_{\text{lim}}^2 \approx g_{\text{peak}}^2$. In Sec. III, we shall use simulations performed at $g^2 = g_{\text{peak}}^2$ to explore the strong-coupling limit and find evidence for a chiral symmetry restoring phase transition at a well-defined N_{fc}.

Writing action (9) in the form $\bar{\chi}_i M_{ij} \chi_j$, it is possible to integrate out the fermion fields analytically to yield the path integral

$$\mathcal{Z}_{\text{latt}} = \int \mathcal{D}V (\det M[V;m])^N. \tag{12}$$

Techniques to simulate the physics described by Eq. (12) typically proceed by evolving a boson configuration $\{V\}$ through a fictitious simulation time using a quasi-Hamiltonian dynamics in which quantum effects are incorporated via periodic stochastic refreshments. We implement this using the hybrid molecular-dynamics (HMD) algorithm.[12] The key step in the evolution involves the calculation of a force,

$$-\frac{\delta S}{\delta V} = N \text{tr} M^{-1} \frac{\delta M}{\delta V}. \tag{13}$$

Since the force can be calculated for arbitrary N, it is possible to simulate the dynamics for noninteger N, which is equivalent to regarding path integral (12) as the fundamental definition of the model. Of course, only for integer N, and therefore, for even integer N_f, is it possible to express the theory as a local action in the fermion variables $\chi, \bar{\chi}$.

In the simulations described in this paper we used a HMD algorithm to perform simulations with arbitrary N_f. In principle, this method is not exact in the sense that results have a systematic dependence on the discrete time step $\Delta\tau$ used to integrate the HMD equation of motion. We have used $\Delta\tau = 0.0025$ on the smallest systems (16^3, 24^3, 32^3), $\Delta\tau = 0.001\,25$ on $16^2 \times 48$, and $\Delta\tau = 0.000\,625$ on $16^2 \times 64$; in all cases we checked that the resulting systematic error is smaller than the statistical error. The mean trajectory length $\bar{\tau} = 1.0$ and $\langle\bar{\chi}\chi\rangle$ are measured using ten stochastic estimators after every trajectory. Roughly 200–400 trajectories were generated for $16^2 \times 48$, 64, and 600 for 24^3 and 32^3, and $O(1000)$ for 16^3. Further details of the numerical methods used can be found in Refs. 8 and 9.

III. RESULTS

We performed simulations on system volumes $L_s^2 L_t = 16^3$, 24^3, and 32^3 using fermion masses $m = 0.01, \ldots, 0.04$. Because action (9) does not treat spacelike and timelike directions equivalently, we also found it useful to explore the consequences of independently varying L_s and L_t, and thus, in addition studied $16^2 \times 48, 64$; $24^2 \times 32, 48$; and $32^2 \times 24$. As we shall see, the anisotropic nature of the model dynamics results in the systematic effects due to finite L_t being much more important than those due to finite L_s. The only observable discussed in this initial study is the chiral condensate $\langle\bar{\chi}\chi\rangle \equiv \langle \text{tr} M^{-1} \rangle$.

A. Strong coupling limit

As described above, to explore the strong-coupling limit $g_R^2 \to \infty$ we made the *ansatz* $g^2 = g_{\text{peak}}^2$, where g_{peak}^2 denotes the

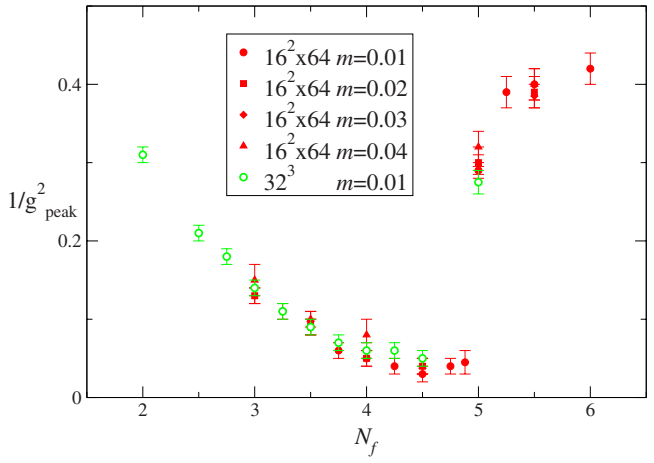

FIG. 2. (Color online) $1/g^2_{\text{peak}}$ vs N_f.

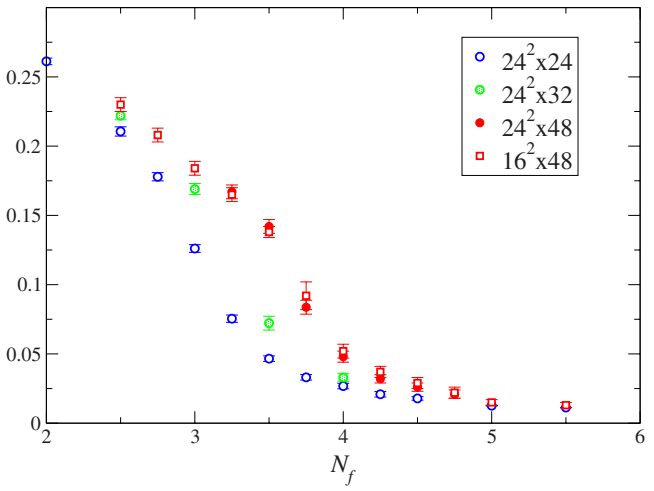

FIG. 3. (Color online) $\langle\bar{\chi}\chi\rangle$ vs N_f at $m=0.01$ on various lattice volumes.

location of the peak in $\langle\bar{\chi}\chi\rangle$ at given N_f. Figure 2 shows $1/g^2_{\text{peak}}(N_f)$ for some representative lattice volumes and fermion masses, confirming that its value (arising as it does from UV lattice artifacts) is (to good approximation) volume and mass independent. The behavior is qualitatively similar to that found for the strong-coupling Thirring model shown in Fig. 3 of Ref. 10. We see that $1/g^2_{\text{peak}}$ decreases as N_f increases from 2 to 4.75, at which point the curve reaches a minimum. There is then a steep increase at $N_f \approx 4.9$ followed by a leveling off, implying a significant change in the model strong-coupling behavior. Our interpretation, to be supported below by a study of the equation of state, is that for N_f below the change the model is in a chirally broken phase and that above the change chiral symmetry is restored, implying $\lim_{m\to 0}\langle\bar{\chi}\chi\rangle=0$. Using this criterion we identify the critical flavor number for chiral symmetry restoration in the strong-coupling limit, with a conservative error, as

$$N_{fc} = 4.8(2). \tag{14}$$

In the rest of this section we analyze data taken at $g^2=g^2_{\text{peak}}$ in an attempt to determine the critical equation of state $\langle\bar{\chi}\chi(m,N_f)\rangle$ in the strong-coupling limit. Note that typically four to six independent simulations were used to identify g^2_{peak} for each N_f. In the thermodynamic zero-temperature limit, a simple *ansatz* for the approximate scaling behavior close to a quantum critical point is given by

$$m = A(N_f - N_{fc})\langle\bar{\chi}\chi\rangle^p + B\langle\bar{\chi}\chi\rangle^\delta, \tag{15}$$

where $\langle\bar{\chi}\chi\rangle|_{N_f=N_{fc}} \propto m^{1/\delta}$ and the conventional exponent in $\langle\bar{\chi}\chi\rangle|_{m=0} \propto (N_{fc}-N_f)^\beta$ for $N_f<N_{fc}$ is given by $\beta=(\delta-p)^{-1}$. We must, however, take account of the fact that our data are taken on finite systems. Figure 3 shows data for $m=0.01$ from various lattices: a comparison between $16^2\times 48$ and $24^2\times 48$ demonstrates that the dominant finite-volume effects are due to varying L_t, while the effects of finite L_s are negligible for $L_s \geq 16$.

The theory of finite-volume effects in models such as Eq. (9) with anisotropic correlations is outlined in Ref. 13. Near a critical point it is possible, in principle, to distinguish two correlation lengths ξ_s and ξ_t, each diverging with a distinct critical exponent ν_s or ν_t as $N_f \to N_{fc}$. In d spacetime dimensions these are related to conventionally defined exponents governing scaling of the order parameter and its associated susceptibility via a generalized hyperscaling relation

$$\nu_t + (d-1)\nu_s = \gamma + 2\beta. \tag{16}$$

Motivated by Fig. 3, in our analysis we take a pragmatic approach and assume all volume effects are due to finite L_t. The *ansatz* for the modified equation of state, inspired by a renormalization-group analysis,[8] is then

$$m = A[(N_f - N_{fc}) + CL_t^{-1/\nu_t}]\langle\bar{\chi}\chi\rangle^p + B\langle\bar{\chi}\chi\rangle^\delta; \tag{17}$$

we fit this form to our data set with a least-squares fit. Our complete data set contains 124 data taken at various N_f, m, L_s, and L_t (recall that the value of $1/g^2_{\text{peak}}$ must be independently determined for each parameter set, so the simulation effort involved is considerable; approximately 100 000 processor hours using 2.4 GHz Opterons were required).

Experience with previous models shows that the fitted equation of state is very sensitive to assumptions made about the scaling window (i.e., the ranges of N_f and m included in the fit), and the smallest volume included in the scaling *ansatz* (17). For this reason we judge that it is best to present a compilation of different fits in Table I. We tried fits to both the "power" equation-of-state (15), with five free parameters, using data from a single lattice size $16^2\times 64$ and fits using the finite-L_t FVS scaling form (17) with seven free parameters. (Note that it is not possible to use hyperscaling to constrain the value of υ_t as done in Refs. 8–10.) In the latter case data with $N_f \geq 5$ were excluded from the fit because their small error bars destabilized the fits; since this data probably come from the chirally symmetric phase, there may be a small systematic error in the identification of g^2_{peak} across the transition.

Fits to Eq. (15) favor $N_{fc} \simeq 3.8$–4 and $p \simeq 0.9$. These values are also favored by the most comprehensive FVS fit to the 96 data points with $N_f<5$. There is no evidence that discarding $m=0.01$ data, which may be most prone to finite-volume artifacts, improves any of the fits. On the other hand, discarding $L_t=16$ and perhaps $L_t=24$ does have a significant

TABLE I. Various fits to the equations-of-state (15) power and (17) "FVS."

Fit	# data	A	B	N_{fc}	δ	p	C	ν_t	χ^2/dof
Power	28	0.31(3)	41.5(15)	3.81(3)	3.96(3)	0.87(3)			4.8
Power, $m \geq 0.02$	18	0.30(7)	87(55)	3.87(9)	4.4(4)	0.82(6)			5.9
Power, $m \geq 0.03$	12	2.1(10)	3800(18)	4.3(1)	6.0(1)	1.3(1)			6.4
FVS, $m=0.01$	53	1.5(7)	63(22)	4.60(15)	3.9(1)	1.3(1)	9.7(10)	1.7(2)	4.0
As above $L_t \geq 24$	48	4.5(32)	161(97)	4.95(16)	4.0(1)	1.6(2)	7.9(5)	2.1(2)	4.0
As above $N_f < 4.5$	46	712(100)	$2.3(3) \times 10^4$	4.46(9)	5.25(4)	3.00(4)	15(3)	1.2(1)	5.4
FVS, all m	96	0.23(1)	19(2)	3.85(4)	4.03(8)	0.88(1)	17.5(17)	1.10(5)	6.3
As above $L_t \geq 32$	70	0.20(1)	10.5(1)	4.7(3)	3.6(1)	0.82(2)	6.0(6)	2.6(8)	5.1
As above $N_f \geq 3$	60	0.21(1)	237(106)	4.6(7)	5.5(3)	0.86(2)	8.1(34)	2.1(1.1)	3.1
$N_f \geq 3$ $L_t \geq 24$	75	0.21(1)	352(137)	4.1(1)	5.8(2)	0.87(2)	15(4)	1.3(2)	3.4
FVS, $m \geq 0.02$	43	0.19(2)	10.4(18)	3.76(11)	3.55(13)	0.78(3)	24(15)	0.9(2)	7.3
As above $L_t \geq 32$	32	0.16(2)	6.5(14)	3.9(4)	3.21(15)	0.72(4)	12(19)	1.2(9)	6.4

effect on the fitted values of N_{fc}, p, and ν_t in the FVS fits. In these cases the fitted $\delta \approx 4$. However, once data with extremal values of N_f are excluded, on the assumption that they lie outside the scaling window, the fitted values of δ rise to $\gtrsim 5$. In almost all cases the fitted value of ν_t exceeds 1, although often not by a statistically significant margin.

Our favorite fit, yielding the smallest χ^2/dof, emerges from the 60 data points with $N_f \in [3,5)$ and $L_t \geq 32$. Another reason for preferring this is that the fitted N_{fc} is consistent with value (14) coming from the behavior of $g^2_{\text{peak}}(N_f)$, which could be regarded as an additional constraint on the global fit. The fit is plotted in Fig. 4 in terms of the control parameter in the thermodynamic limit $N_f' = N_f + CL_t^{-1/\nu_t}$, so that data with differing L_t should collapse onto a single curve for each value of m.

To summarize: this "best" fit provides a reasonable description of the data in the window $4.5 \lesssim N_f' \lesssim 6$, in particular for the smallest mass $m=0.01$; fits of form (17) are capable of yielding a fitted N_{fc} consistent with Eq. (14); and the preferred value of $\nu_t \approx 2$ once this consistency criterion is applied.

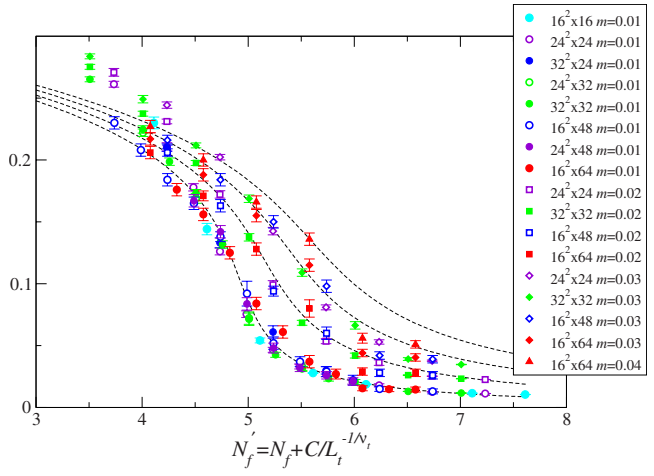

FIG. 4. (Color online) Finite volume scaling fit to Eq. (17) to data with $m=0.01$ (circles), 0.02 (squares), 0.03 (diamonds), and 0.04 (triangles) in terms of N_f'.

B. $N_f=2$

Next we turn our attention to the physical case $N_f=2$. Since $N_{fc} > 2$, we expect chiral symmetry to be broken at strong coupling and potentially restored at some finite g_R^2. This transition has been studied using renormalization-group methods in Ref. 14. Accordingly we study $\langle \bar{\chi}\chi \rangle$ as a function of $1/g^2$. Our results are summarized in Fig. 5.

As before, we have attempted to fit a critical equation of state using form (15) to data from $16^2 \times 64$ and form (17) in each case replacing $(N_f - N_{fc})$ with $(g^{-2} - g_c^{-2})$. No stable fits were found unless data with $1/g^2 \lesssim 1$ were excluded. Our most comprehensive fit, using the FVS form and restricting the data to $L_t \geq 48$ with $1/g^2 \leq 0.9$, yields $1/g_c^2 = 0.632(6)$ and is shown in the figure. All the fits we found identify a $1/g_c^2 \simeq 0.6 \gg 1/g^2_{\text{peak}}$, but all clearly undershoot the data at weaker couplings by a considerable margin. We conclude that the equation-of-state *Ansätze* (15) and (17) are inadequate to describe the data.

Instead, we will distinguish between a "strong-coupling" regime $1/g^2 \lesssim 0.75$ where $\langle \bar{\chi}\chi \rangle$ is numerically large and finite-volume effects are negligible, and a "weak-coupling" regime $1/g^2 \gtrsim 0.75$ where the opposite holds true. Two com-

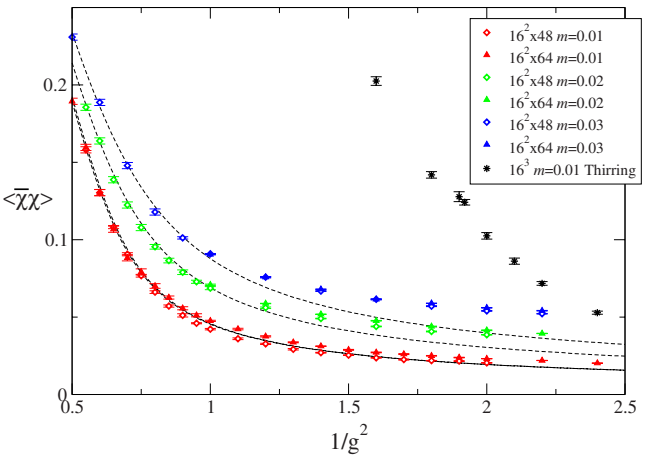

FIG. 5. (Color online) $\langle \bar{\chi}\chi \rangle$ vs $1/g^2$ for $N_f=2$.

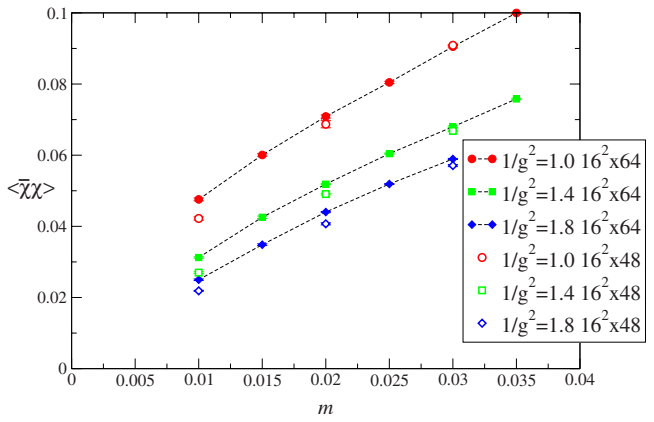

FIG. 6. (Color online) $\langle\bar{\chi}\chi\rangle$ vs m for $N_f=2$ in the weak-coupling regime.

ments about the weak-coupling regime are worth making. First, as is clear from Figs. 5 and 6, finite-volume effects are unexpectedly large and indeed increase in relative importance until $1/g^2 \gtrsim 1$; it is this feature that has made a global FVS fit impossible. In a conventional symmetry-breaking scenario, by contrast, one expects the finite-volume effects to be larger in the broken phase, where there are long-range correlations due to Goldstone bosons. Second, in a chirally symmetric phase one expects $\langle\bar{\chi}\chi\rangle \propto m$ for small m and weak interactions; inspection of the data plotted in Fig. 6 appears to imply either that a linear extrapolation to $m \to 0$ would yield a nonvanishing order parameter, or alternatively, that chiral symmetry restoration for these values of $g^2 < g_c^2$ would require $\langle\bar{\chi}\chi(m)\rangle$ to exhibit some negative curvature, for which there is some tentative evidence in the figure. We conclude that either chiral symmetry remains broken at weak coupling or that there are long-range correlations in this region.

We briefly consider alternative scaling scenarios. In the chiral and thermodynamic limits two other kinds of behavior are possible to envisage and are not currently excluded by our data. First, a form $\langle\bar{\chi}\chi\rangle = Ae^{-B/g^2}$ would predict broken chiral symmetry for all g^2. This is barely credible since the $\chi-\bar{\chi}$ forces in this model are weaker than for the $N_f=2$ Thirring model, where two independent simulation studies find a second-order chiral restoring transition at $1/g^2 \simeq 1.9$ (Refs. 8 and 15) [Fig. 5 also shows Thirring data from 16×10^3 (Ref. 8)]. Second, $\langle\bar{\chi}\chi\rangle = Ae^{-B/(g_c^{-2}-g^{-2})^q}$ describes chiral symmetry restoration via an infinite order phase transition at $g^2=g_c^2$. Without a reliable finite-volume scaling hypothesis we cannot estimate g_c^2, B, or q. By analogy with the Kosterlitz-Thouless transition in $2d$ systems, though, this scenario predicts a critical, and hence, strongly fluctuating system for $g^2 > g_c^2$ which could plausibly account for the observations reported above. A similar scenario is predicted under certain circumstances in Ref. 16.

IV. DISCUSSION

In this paper we studied model (6) which has very similar properties, including the same global symmetries, as the graphene-related model recently proposed to describe quantum critical behavior in the (N_f, e^2) plane.[5] Using a simulation strategy devised for the $2+1d$ Thirring model,[10] we have identified the critical number of flavors separating insulating from conducting phases in the strong-coupling limit to be $N_{fc}=4.8(2)$. This implies that the strong-coupling limit of graphene with $N_f=2$ is an insulator. Since the properties of a critical point should be universal, we expect this result to be a robust prediction of our work, thus, furnishing the first systematic nonperturbative prediction of quantum critical behavior in this system. We also managed a reasonable fit of our strong-coupling data to an equation of state describing a continuous phase transition at the critical point and obtained estimates for the critical exponents.

The fitted value of ν_t gives partial information about the nature of correlations in the vicinity of the fixed point. Substituting our favored values $\delta=5.5$, $p=0.86$, and $\nu_t=2.1$ into Eq. (16), we obtain $\nu_s=\frac{1}{2}\gamma-0.83$. Without studying the order-parameter susceptibility we have no independent estimate of γ, but note that it would need to have a value of $O(6)$ in order for ν_s to exceed ν_t. Now, there is a further relation governing the scaling of critical correlation functions,[13]

$$(d-2+\eta_t)\nu_t = (d-2+\eta_s)\nu_s \Rightarrow \frac{\nu_t}{\nu_s} = \frac{1+\eta_s}{1+\eta_t}, \qquad (18)$$

where order-parameter correlations $\langle\bar{\chi}\chi(0)\bar{\chi}\chi(x_{s,t})\rangle \propto x_{s,t}^{-\eta_{s,t}}$ at criticality with the exponent taking the appropriate value depending on whether the displacement x is timelike or spacelike. The ratio $\eta_s/\eta_t > 1$ if $\nu_s/\nu_t < 1$ and vice versa. However, η_s/η_t may be identified with the dynamical critical exponent z characterizing the quantum critical point, in the sense that the dynamics remains invariant under the scale transformation $\vec{x} \to \ell\vec{x}$; $x_0 \to \ell^z x_0$. By considering the anomalous dimension of the Fermi velocity using the $1/N_f$ expansion, Son[5] obtained $z<1$, which has implications for the stability of the quasiparticle excitations. If we assume that the same critical exponent governs both quasiparticle and order-parameter correlations, then reconciling the two calculations requires an unusually large value of γ.

Next, we set N_f to the physical value 2 and studied the chiral order parameter as a function of coupling strength. Here our results are harder to interpret; we observe a crossover from strong- to weak-coupling behavior at $1/g^2 \simeq 0.75$ but were unable to model the equation of state, leaving the nature of the weak-coupling regime unclear. There is evidence, both from the large finite-volume effects and the curvature in $\langle\bar{\chi}\chi(m)\rangle$, for strong correlations. Work is currently in progress to study the quasiparticle propagator in order to explore the dispersion relation and expose any quantum critical behavior from an independent direction, and also to further investigate the nature of the fluctuations in the weak-coupling phase at $N_f=2$.

ACKNOWLEDGMENTS

S.J.H. thanks the Galileo Galilei Institute for Theoretical Physics for hospitality and the INFN for partial support during the completion of this work.

[1] K. S. Novoselov, A. K. Geim, S. V. Morozov, D. Jiang, M. I. Katsnelson, I. V. Grigorieva, S. V. Dubonos, and A. A. Firsov, Nature (London) **438**, 197 (2005).
[2] G. W. Semenoff, Phys. Rev. Lett. **53**, 2449 (1984).
[3] V. P. Gusynin, S. G. Sharapov, and J. P. Carbotte, Int. J. Mod. Phys. B **21**, 4611 (2007).
[4] M. Creutz, J. High Energy Phys. 04 (2008) 017.
[5] D. T. Son, Phys. Rev. B **75**, 235423 (2007).
[6] D. V. Khveshchenko, Phys. Rev. Lett. **87**, 246802 (2001); E. V. Gorbar, V. P. Gusynin, V. A. Miransky, and I. A. Shovkovy, Phys. Rev. B **66**, 045108 (2002).
[7] J. E. Drut and D. T. Son, Phys. Rev. B **77**, 075115 (2008).
[8] L. Del Debbio, S. J. Hands, and J. C. Mehegan, Nucl. Phys. B **502**, 269 (1997).
[9] L. Del Debbio and S. J. Hands, Nucl. Phys. B **552**, 339 (1999); S. J. Hands and B. Lucini, Phys. Lett. B **461**, 263 (1999).
[10] S. Christofi, S. J. Hands, and C. Strouthos, Phys. Rev. D **75**, 101701(R) (2007).
[11] C. J. Burden and A. N. Burkitt, Europhys. Lett. **3**, 545 (1987).
[12] S. A. Gottlieb, W. Liu, D. Toussaint, R. L. Renken, and R. L. Sugar, Phys. Rev. D **35**, 2531 (1987).
[13] K. Binder and J.-S. Wang, J. Stat. Phys. **55**, 87 (1989).
[14] I. F. Herbut, Phys. Rev. Lett. **97**, 146401 (2006); O. Vafek and M. J. Case, Phys. Rev. B **77**, 033410 (2008).
[15] I. M. Barbour, N. Psycharis, E. Focht, W. Franzki, and J. Jersák, Phys. Rev. D **58**, 074507 (1998).
[16] D. V. Khveshchenko and W. F. Shively, Phys. Rev. B **73**, 115104 (2006).